

Physics laboratory -LM, A.A. 2021/22

Group: 5

Cohort: 1

Experience date: 27-28/10 and 2/11, 2021

Delivery date: 11-11-2021

Giovanni Celotto 2052372 giovanni.celotto@studenti.unipd.it

Andrea Pompermaier 2053046 andrea.pompermaier@studenti.unipd.it

Massimo Colombo 2056104 massimo.colombo@studenti.unipd.it

Cristian Tibambre 2054971 cristiandavid.tibambreheredia@studenti.unipd.it

Study of the Compton Scattering

1 Introduction

Compton scattering is the principal process of photon interaction with matter for energies that vary from 100 keV to some MeV. This phenomenon was firstly described by Compton in 1922 and it was one of the first proofs of the quantum behaviour of light. The energy of the scattered photon $E_{\gamma'}$ at an angle θ with initial energy E_{γ} , diffused by a free and at rest electron, follows the next relation:

$$E_{\gamma'} = \frac{E_{\gamma}}{1 + \frac{E_{\gamma}}{m_e c^2} (1 - \cos\theta)} \quad (1)$$

The differential cross section of the process was described by Klein and Nishina in 1929:

$$\frac{d\sigma}{d\Omega} = \frac{r_e^2}{2} \left(\frac{E_{\gamma'}}{E_{\gamma}} \right)^2 \left(\frac{E_{\gamma'}}{E_{\gamma}} + \frac{E_{\gamma}}{E'_{\gamma}} - \sin^2\theta \right) \quad (2)$$

where $r_e = \frac{e^2}{4\pi\epsilon_0 m_e c^2} = 2.82 \cdot 10^{-15} m$ is the classical radius of the electron.

2 Objectives

The main purpose of this work consists in the study of Compton scattering of 511 keV photons, produced by a ^{22}Na source and detected by NaI(Tl) scintillators, and in particular of:

- Verification of the Compton scattering relation through the measurement of the energy of the scattered photons at different angles.
- Measurement of the Compton cross section and verification of Klein-Nishina formula.

3 Experimental setup

The experimental setup used for this experiment consists of:

- A ^{22}Na and an ^{241}Am γ -ray sources.
- An oscilloscope Tektronix TBS1000C.

- Three cylindrical NaI(Tl) scintillators (SCIONIX HOLLAND SFQ658) with diameter 7.5 cm and height 7.5 cm connected to photomultipliers (SCIONIX HOLLAND SVE984).
- A lead collimator with a diameter of $\simeq 2\text{cm}$ and a length of $\simeq 8\text{cm}$.
- A cylindrical aluminum sample used as a scatterer for the differential cross section measurement with diameter $d_{Al} = (3.5 \pm 0.1)\text{cm}$ and height $h_{Al} = (8 \pm 1)\text{mm}$.
- Nuclear Instrument Modules (NIMs) formed by: a Power Supply (CAEN N1470) which operates at HV = +600 V; a Quad Linear Gate FAN-IN-FAN-OUT (Philips 744); a CFTD (INFN Pd); a Logic Unit (SEN LU278); a scaler (CAEN N145).
- A digitizer (CAEN DT5720) 250 MS/s 12bit.
- A computer which uses VERDI acquisition system.

The ^{22}Na source is put inside the lead collimator between the Tagger and the Scatterer to obtain an incoming photon beam with a properly defined geometry. A certain fraction of ^{22}Na decays β^+ to ^{22}Ne producing a positron which quickly annihilates with an electron and emits two photons of 511 keV in opposite directions (due to the four-momentum conservation). The coincidence signals of 511 keV photons recorded by the three detectors are used to select the scattering events. After the Scatterer, there is a rotating metallic bar above which the Detector can be placed in an arbitrary position. The workbench has notches that denote the angular position of the Scatterer-Detector direction concerning the Tagger-Scatterer one: they vary from 0° to 90° with steps of 10° . The detected signals are then collected and analyzed by the front-end electronic system and the spectra, recorded by the detectors, can be visualized run-time in the computer.

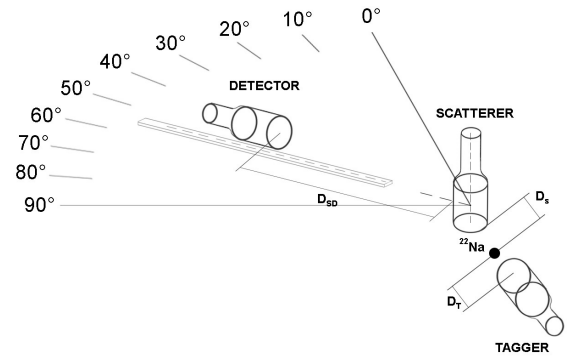


Figure 1: Illustration of the experimental setup
The calibration procedure is the same for each detector:

- The output signal of each photomultiplier is sent to the Quad Linear Gate where it is duplicated. One of the output is directed to the digitizer, which record the spectrum, instead the other is connected to the CFTD to select the events. The output signals which come from the photomultiplier are negative and they present a fast linear fall time with a time width of $\sim 30\text{ns}$, a maximum amplitude (for signals of 511 keV photons) of $\sim 560\text{keV}$ and an exponential rise time with duration $\sim 500\text{ns}$. The noise level is $\sim 25\text{mV}$. The scaler can be used to measure the counting rate of the detectors which typically varies from 1 kHz to 10 kHz (in the configuration at 0°) depending on their distance to the source.
- The CFTD threshold can be modified via a trimmer adjustable with a screwdriver. In order to set it, we observed in the oscilloscope the effect of different thresholds in the output signal of the detector. The correct threshold is the minimum value necessary to cut the electronic noise.

- The width and the delay of CFTD can be modified using microswitches. We set the delayed output signals of CFTD to have a width of $\sim 100\text{ns}$ and partial overlaps of the three detectors signals (this procedure is carried out with the oscilloscope).
- The coincidences of more than one detector can be taken by connecting the CFTD outputs to the Logic Unit and selecting the number of simultaneous signals that must be acquired.

4.1 Energy calibration

The calibration of the detectors is fundamental to correctly measure the energy of the scattered photons and electrons in the following analysis. For this scope, we recorded for each detector an energy spectrum of two sources: ^{22}Na and ^{241}Am . We measured the energy, in arbitrary units of the digitizer, of 511 keV and 1275 keV from ^{22}Na and 59 keV from ^{241}Am . The energies, expressed in arbitrary units, have been fitted to the nominal energies: $E[\text{a.u.}] = p_0 + p_1 \cdot E[\text{keV}]$

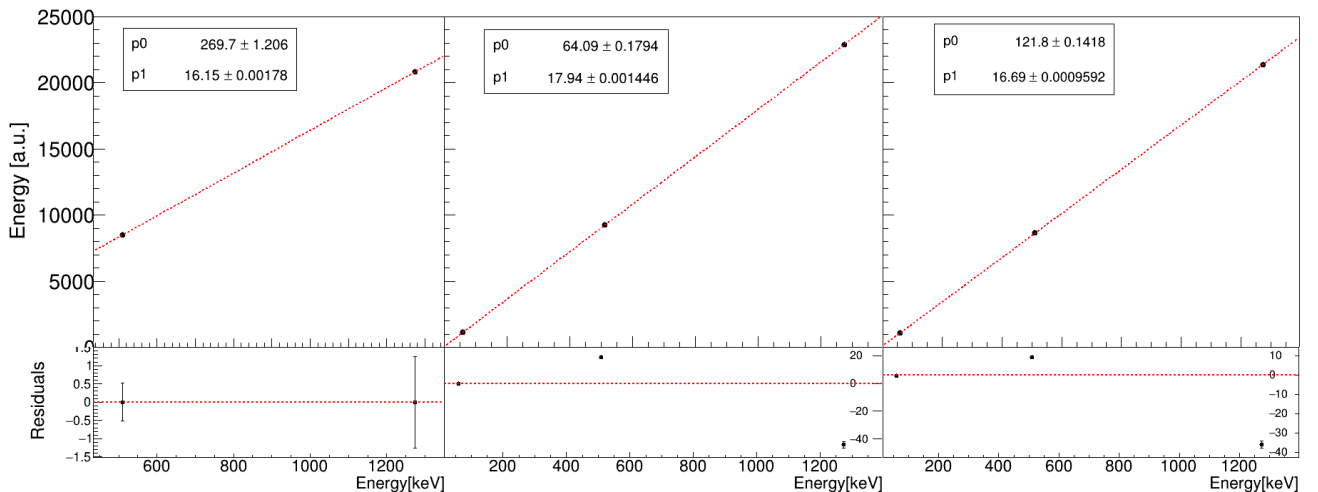


Figure 2: Calibration fit results for: Tagger (left), Scatterer (center), Detector (right).

Detector	E_{59} [a.u.]	E_{511} [a.u.]	E_{1275} [a.u.]	p_0 [a.u.]	p_1 [a.u./keV]
T	-	8509 ± 1	20850 ± 1	250.8 ± 1.2	16.160 ± 0.002
S	1132.0 ± 0.1	22880 ± 2	92248 ± 1	64.1 ± 0.2	17.940 ± 0.001
D	1116.0 ± 0.1	8662.0 ± 0.6	21360 ± 2	121.8 ± 0.1	16.690 ± 0.01

Table 1: Energy calibration results. The 59 keV peak of ^{241}Am in the Tagger was not considered since it was only partially detected because of the high threshold.,

4.1.1 Tagger F(511)

The Tagger is used in coincidence with the other detectors to select the 511 keV photons. Moreover, it can be used to determine the fraction F(511) of 511 keV photons fully releasing their energy into the Detector. This parameter will be necessary to estimate the intensity of incident photons in the Scatterer (Sec. 7.2). The following equation is used to obtain the value of F(511).

$$\frac{A(511)}{A_{tot}} = F(511) \quad (3)$$

$A(511)$ is the area of the peak at 511 keV and A_{tot} is the total number of events that make up the spectrum. The number of events recorded in the Tagger are $A_{tot} = (1.368 \pm 0.001) \cdot 10^6$ (Poisson statistics) and by fitting with a Gaussian added to a polynomial background, we obtain the area under the curve $A_{511} = (5.091 \pm 0.009) \cdot 10^5$.

$$F(511) = (37.23 \pm 0.06)\% \quad (4)$$

4.2 Relationship between the precision of the peak and statistics

It is possible to evaluate the relation between the relative uncertainty of the peak position and the number of events detected. The relative errors of the 511 keV peak centroids have been fitted concerning the number of entries in the spectrum using the function $y = \frac{p_0}{\sqrt{x}}$. From the results (Fig. 3) we understood that, in order to have a good precision for the peak estimation (better than 0.001) we had to record spectra with statistics of at least 10000 events.

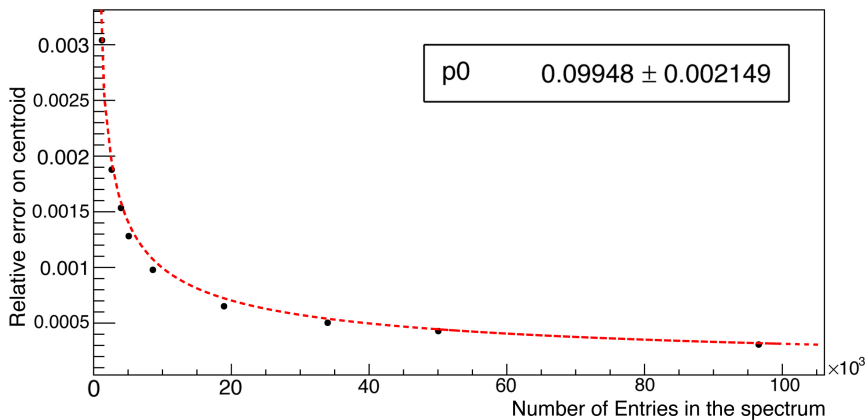


Figure 3: Relative uncertainties of 511 peak position with respect to the total number of events.

5 Definition of the measurement geometry

The geometry of the experimental setup plays a key role in the comprehension and interpretation of the results. The experimental measurements are the following:

- Distance Tagger-Source: $d_{Ts} = (4.0 \pm 0.5)cm$.
- Distance Source-Scatterer: $d_{Ss} = (5.0 \pm 0.5)cm$.
- Distance Source-Scatterer: $d_{DS} = (31.0 \pm 0.5)cm$ (for the measurement of the energy of scattered photons) and $d_{DS} = (33.0 \pm 0.5)cm$ (for the measurement of the cross section).

5.1 Geometry definition and photon interaction model

Let's analyze the actual angle ϕ of deviation of a generic photon emitted by the source and scattered due to the Compton effect, in our experimental setup. ϕ depends on the incidence position in the Scatterer (C in Fig. 4), and on the Detector's point where the scattered photon γ' is absorbed.

First consider the angle β that a photon emitted by the source has, with respect to the direction indicated by the collimator. The maximum angle β_{max} for which a photon can reach the Scatterer without being shielded by lead can be estimated geometrically by knowing the diameter of the hole in the lead ($d_h \simeq 2\text{cm}$) and its depth ($h_h \simeq 4\text{cm}$). We obtain $\beta_{max} \simeq 14^\circ$. Known the angular interval $[-\beta_{max}, \beta_{max}]$ and the distance between the Scatterer and the collimator ($D_{h-S} \simeq 1.5\text{cm}$), it is recognized in the yellow intersection (Fig. 4), the region of interaction between incident photons γ and electrons of the material. It must be observed that the probability of a photon to be scattered at any point of the intersection follows the relation: $p(x) = Ne^{-\mu x}$, where μ is the linear attenuation coefficient, N is a normalization constant and x is the length of its path in the material. For NaI(Tl), the linear attenuation coefficient at $\sim 511\text{keV}$ is about $\mu_{NaI} \sim 0.26\text{ cm}^{-1}$.

From geometrical considerations the length of the chord which will be used in the next session was estimated to be:

$$\overline{AB}(\beta) = 2 \frac{\sqrt{[1 + \cot^2(-\beta)](\frac{d_s}{2})^2 - (h_h + D_{h-S} + \frac{d_s}{2})^2}}{\sqrt{(1 + \cot^2(-\beta))}} \quad (5)$$

Given the point C where the photon γ scatters against an electron, we want to estimate the minimum and maximum deviation angles φ to the vertical, that γ' photon can have to be absorbed by the Detector. To do this, we set our coordinate reference system as shown in Fig. 4, and we calculated the positions of the edges of the Detector E and F, as a function of the nominal angle θ , and the coordinates of point C, as a function of the angle β and the length \tilde{X} . We must observe that the position of the center Z with respect to which the Detector rotates and for which we consider the angle θ does not coincide with the center of the Scatterer. A vertical translation of $D_{OZ} \simeq 1.6\text{ cm}$ was measured. This shift has been considered to define the coordinates of E and F. Given these coordinates, it is possible to calculate the angles φ_{min} and φ_{max} for a generic point C in the intersection:

$$\varphi_{min} = \arctan\left(\frac{C_x - E_x}{E_y - C_y}\right) \quad \varphi_{max} = \arctan\left(\frac{C_x - F_x}{F_y - C_y}\right)$$

In this way, the angle φ of deviation to the vertical axis for which a photon is absorbed by the Detector has to be within φ_{min} and φ_{max} . To conclude the actual angle of deviation ϕ of an incident photon due to the Compton effect in our experimental setup results equal to $\phi = \varphi - \beta$.

5.2 Estimation of statistical and systematic errors in angular positions with Monte Carlo simulation

The model described in the previous section has been implemented using a Monte Carlo simulation. The algorithm works in this way:

- A photon with an angle $\beta \in [-\beta_{max}, \beta_{max}]$ is produced with a uniform probability density.

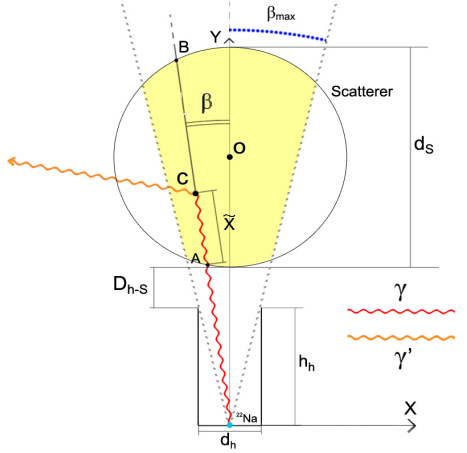


Figure 4: Scatterer geometry

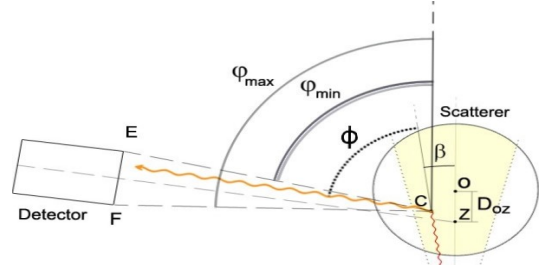


Figure 5: Source-Detector geometry

- For each angle β selected there is a certain cord $\overline{AB}(\beta)$ which is the maximum path inside the Detector and it is used to normalize the probability distribution of interaction with matter. In this range, an interaction point \tilde{X} is generated with the exponential law¹.
- In \tilde{X} a scattered photon is produced by using the probability distribution of Klein Nishina (Eq. 2) with an angle ϕ with respect to the incoming direction.
- Knowing the position of the Detector, which in this case is modeled as a segment of length 7.5 cm at the distance d_{DS} to the edges of the Scatterer, for each angular position of the movable arm (θ) we set the following conditions to accept an event: the angle of emission with respect to the vertical direction has to be within the range $[\varphi_{min}, \varphi_{max}]$. (Fig. 5)
- The accepted events for each nominal angular distribution have been recorded in a histogram. (Fig. 6)

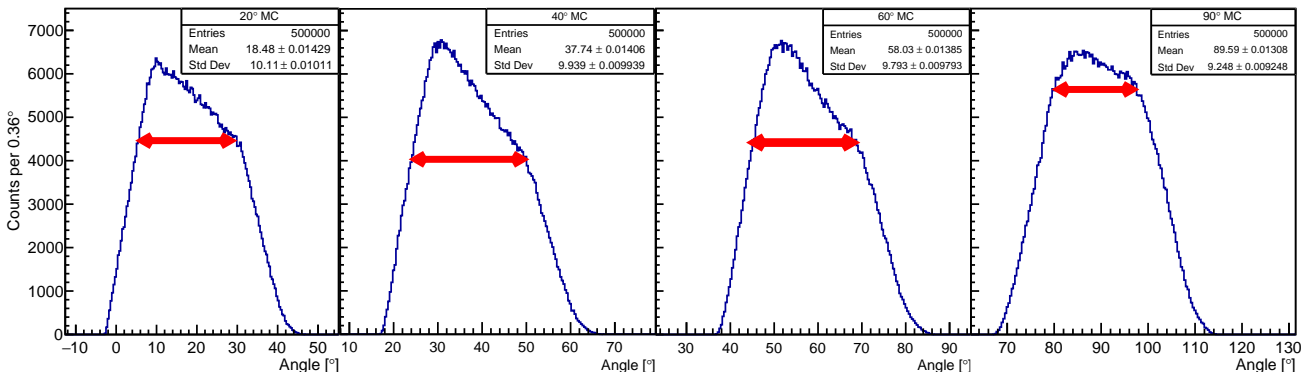


Figure 6: Monte Carlo simulations of angular distribution for each experimental configuration. The red lines indicate the estimated statistical errors.

From each simulation, it is possible to obtain an estimation of the mean angle of emission. We considered the mean and not the maximum value because we know that it is a simple model which can not reproduce exactly the 3D geometry. It is reasonable that in a 3D model the middle values have a major weight. In general, the photons with lower angles are favored (Eq. 2) and so the main angles detected are typically lower than the nominal ones. Moreover, for each angular position θ , the simulation allows us to estimate the range of the effective deviation angles that the photons may have when measured by the Detector in our experimental configuration. These uncertainties, indicated in Fig. 6 with red lines, are asymmetric respect to the nominal value: this fact is physically consistent with the Klein-Nishina formula.

6 Measurement of energy of the scattered photon

After setting the coincidence of the three detector signals, we recorded the spectra of Detector and Scatterer for different angular positions: 20°, 40°, 60°, 90°. The configuration with 0° has been recorded but not considered in this analysis since there was too much noise: there are a lot of 511 keV photons that interact with the Scatterer in coincidence with other photons that can be revealed by the Detector. The duration of the acquisitions has been chosen to have enough statistics. From the considerations of Sec. 4.2, we decided to acquire spectra with statistics greater than 10000 events. To improve the analysis the recorded spectra have been filtered by selecting the events which satisfy the next conditions:

¹The linear attenuation coefficient previously mentioned refers only to the Compton scattering

- The energy of the Tagger event must be lower than 600 keV: this means that the event probably corresponds to a 511 keV photon which can be completely absorbed by the Tagger or it can only partially interact with it (through Compton scattering).
- The energy of the Scatterer event must be lower than 450 keV. This is the range in which we expect the energy of scattered electrons.
- The sum of the energies of the coincidence events measured in the Detector and in the Tagger must be within the range² of [400 keV, 600 keV].

The filtered spectra present a remarkable peak. Each spectrum has been fitted with a Gaussian fit (in some cases added to a polynomial background) to obtain an estimation of the peak centroid: this value corresponds to the best estimation of the energy of the scattered photons (Detector) or electrons (Scatterer) for each angular position. The results are summarized in the next plots.

θ	Number of diffused photons	$E_{\gamma'}$ [keV]	E_e [keV]
20°	3609	447.1 ± 0.9	63.1 ± 0.7
40°	2859	422 ± 1	77.5 ± 1
60°	3984	360 ± 1	148 ± 1
90°	31432	280.0 ± 0.4	227.0 ± 0.3

Table 2: Energies of scattered photons and electrons at different angles.

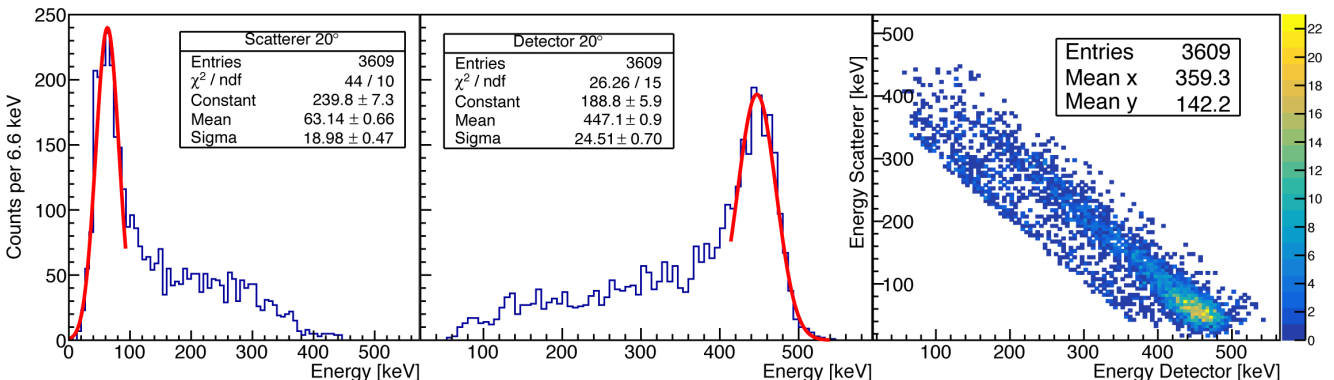


Figure 7: Filtered spectra of Scatterer, Detector and Scatterer vs. Detector for $\theta = 20^\circ$.

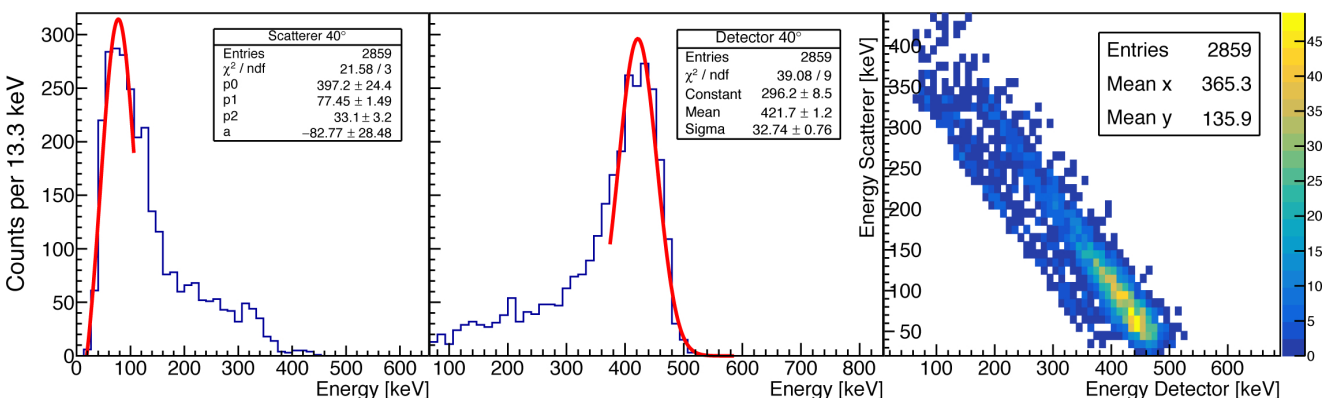


Figure 8: Filtered spectra of Scatterer, Detector and Scatterer vs. Detector, for $\theta = 40^\circ$.

²This range was determined starting from the gaussian tails of the peak

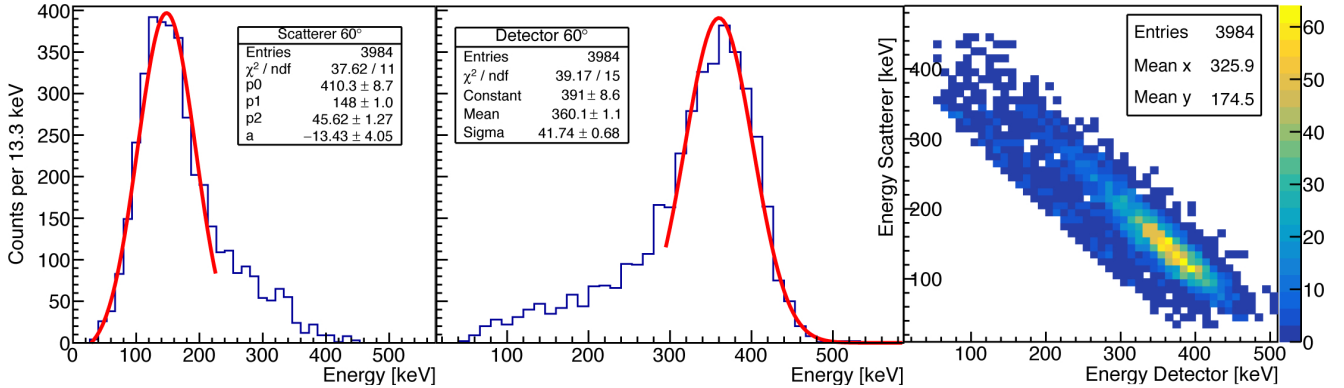


Figure 9: Filtered spectra of Scatterer, Detector and Scatterer vs. Detector for $\theta = 60^\circ$.

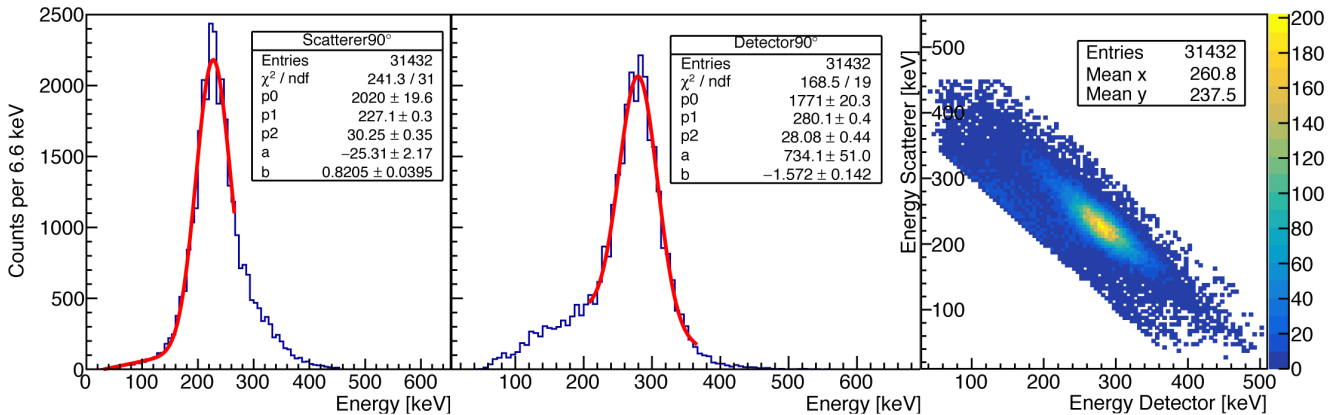


Figure 10: Filtered spectra of Scatterer, Detector and Scatterer vs. Detector, for $\theta = 90^\circ$.

There is a strong correlation between the energy measured in the Detector and in the Scatterer as a consequence of the energy conservation principle. To highlight this fact we fitted the energies of scattered electrons with respect to the energies of scattered photons: $E_e = p_0 + p_1 \cdot E_{\gamma'}$ (Fig. 11). Since the sample at 40° has lower statistics, there is a higher uncertainty in the measure of the centroids of the energy peaks in the Scatterer and Detector. For this reason, we made the same plot without considering that point (Fig 11). The parameter $p_0 = E_{\gamma'} + E_e = (511 \pm 1) \text{ keV}$ confirms the conservation of the energy. Also, the uncertainties associated with the energies (apart for 40°) are likely estimated, as it is possible to see in the residuals plot.

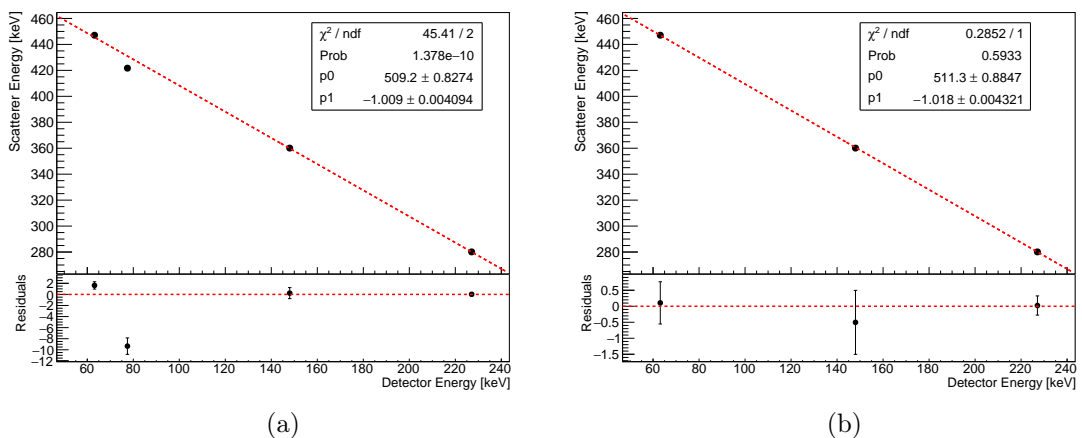


Figure 11: Trend of the energy measured in the Scatterer vs. energy measured in the Detector for each angular position

Now it is possible to plot the energy of scattered photons/electrons as a function of the angle θ in order to verify the experimental agreement of the Compton formula (Eq. 1). The uncertainty associated with the angle σ_θ is the one estimated in section 5.2. The results are shown in Fig.12.

By inverting Eq. 1, it is possible to obtain an estimation of the real observed scattering angle θ_{exp} for each nominal angular position.

$$\theta_{exp} = \arccos \left(2 - \frac{511[\text{keV}]}{E_{\gamma'}[\text{keV}]} \right) \quad \sigma_{\theta_{exp}} = \left(\frac{511[\text{keV}]}{E_{\gamma'}^2[\text{keV}]} \right) \frac{1}{\sqrt{1 - \left(2 - \frac{511[\text{keV}]}{E_{\gamma'}[\text{keV}]} \right)^2}} \sigma_{E_{\gamma'}} \quad (6)$$

These values are compared with those obtained by using the simulation, which are always lower than the nominal ones and cannot completely reproduce the experimental data (Tab. 3).

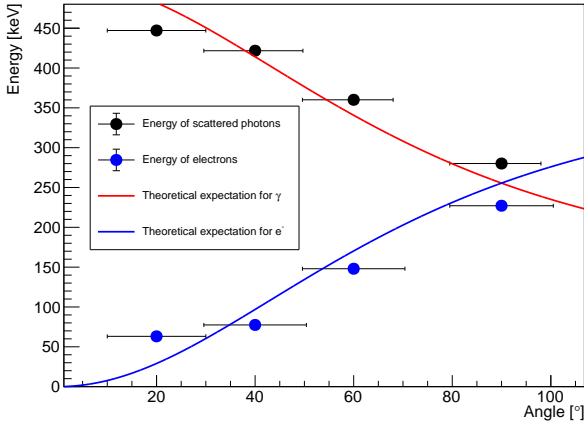


Figure 12: Experimental $E_{\gamma'}$ and E_e compared to theoretical expectations.

Nominal angle	θ_{exp}	θ_{sim}
20°	$(31.0 \pm 0.3)^\circ$	$(18.48 \pm 0.01)^\circ$
40°	$(37.9 \pm 0.3)^\circ$	$(37.74 \pm 0.01)^\circ$
60°	$(54.5 \pm 0.3)^\circ$	$(58.03 \pm 0.01)^\circ$
90°	$(79.9 \pm 0.2)^\circ$	$(89.59 \pm 0.01)^\circ$

Table 3: Comparison of the scattering angles deduced by the experimental results with that obtained using the simulation.

7 Measurement of the Compton cross section

The experimental formula necessary to estimate the differential cross section is:

$$\left[\frac{d\sigma(\Theta_f)}{d\Omega} \right]_{exp} = \frac{\Sigma_\gamma}{\epsilon N \Delta\Omega_f \frac{I}{S_{Al}}} \quad (7)$$

Where Σ_γ is the intensity of the scattered photons in the 511 keV peak, ϵ is the photopic efficiency, N is the number of electrons in the sample, $\Delta\Omega_f$ the solid angle underlined by the Detector and I/S_{Al} is the intensity per unit of surface of the incident photons on the aluminum sample. We set the Detector at $\theta = 90^\circ$ with respect to the incoming photon beam since, for this angle, the cross section is approximately constant and the angular systematic error has a minor contribution. From the geometrical physical information of the Al sample and the Detector position we can directly estimate:

- $\Delta\Omega_f = \frac{S_{det}}{d_{SD}^2} = (0.041 \pm 0.001) \text{sr}$ (where S_{det} is the surface of the Detector);
- The number of electrons in the sample $N = \frac{V \rho_{Al} N_A Z_{Al}}{M_{Al,mol}} = (6 \pm 1) \cdot 10^{24}$ (where V is the volume of the detector, N_A is the Avogadro number, Z_{Al} the atomic number, $M_{Al,mol}$ the molar mass and ρ_{Al} the density of the aluminum sample).

The photopeak efficiency ϵ , the intensity of incident photons per unit of surface $\frac{I}{S_{Al}}$ and the intensity of the scattered photons at $90^\circ \Sigma_\gamma$ are obtained in the next sections through the analysis of the experimental data.

7.1 511 keV photopeak efficiency

The photopeak efficiency of the 511 keV photons corresponds to the fraction of 511 keV that is completely recorded by detectors with respect to the total: $\epsilon = \frac{N_{511}}{N_{tot}}$ (where N_{511} corresponds to the number of events in 511 keV peak and N_{tot} is the total number of 511 keV detected, also partially, by the Detector in coincidence with the Tagger).

We moved the Detector in contact with the lead collimator and we recorded the coincidence spectra of Detector and Tagger. The two spectra contain the 511 keV photons coincidence so we can estimate ϵ by measuring the number of photons in the 511 keV peak of the Detector N_{511} and dividing it by the total number of events recorded by the Tagger N_{tot} :

$$\epsilon = \frac{N_{511}}{N_{tot}} \quad (8)$$

The entries registered in the Tagger are $N_{tot} = (4.156 \pm 0.006) \cdot 10^5$ (Poisson statistics).

To obtain the photons corresponding to 511 KeV, we fit the peak using a gaussian added to a first order polynomial (background), obtaining the effective number of photons in the Detector inside the peak, which are: $N_{511} = (2.820 \pm 0.005) \cdot 10^5$. Applying the Eq. 8 we obtain the efficiency:

$$\epsilon = (67.8 \pm 0.1)\% \quad (9)$$

7.2 Intensity of incident photons

Once the fraction of photons with energy 511 keV $F(511)$ recorded by the Tagger is calculated, it is possible to determine how many of these photons hit the aluminum sample per unit of time. To do this, it is necessary to know how many events have been recorded by the Tagger during a certain time interval. We set an acquisition time of one hour and we measured with the scaler the total number of events ($N_{scaler,tot}$) detected by the Tagger: $N_{scaler,tot} = (2.4196 \pm 0.0005) \cdot 10^7$ (Poisson statistics). It means that the number of events per unit of time in the Tagger is $N_{scaler} = (6.721 \pm 0.001) \cdot 10^3 s^{-1}$. Considering $F(511)$ (Eq. 4) it is possible to deduce the intensity of 511 keV photons which produce a 511 keV peak:

$$I = N_{scaler} \cdot F(511) = (2.502 \pm 0.004) \cdot 10^3 s^{-1} \quad (10)$$

The area of the sample is:

$$S_{Al} = \pi \cdot (d_{Al}/2)^2 = (9.6 \pm 0.5) 10^{-4} m^2 \quad (11)$$

And we get the intensity per unit of surface:

$$\frac{I}{S_{Al}} = (2.6 \pm 0.1) \cdot 10^6 m^{-2} s^{-1} \quad (12)$$

An event is considered accepted if it contributes to the energy photopeak in the ^{22}Na spectrum. Although, low energy photons, interacting with the detectors or the aluminum sample, are recorded as background interactions that are not relevant for the cross section estimation.

7.3 Intensity of scattered photons

It has been recorded an energy spectrum at $\theta = 90^\circ$ for a duration of 12 hours. In order to reduce the noise due to the environmental radiation and to the events that don't come from Compton scattering with the sample, we acquired a background spectrum (same Detector position but without the aluminum sample) for a duration of 57 min and 30 s. Since we are interested in the photons which produce in the Tagger a full photopeak, we filtered the two spectra (with Al sample and background) by considering only the coincidence Tagger-Detector due to events that have an energy in the Tagger in the range [400 keV, 600 keV]. Then the background spectrum (re-scaled to 12 hours) has been subtracted to that recorded with the aluminium sample. Finally it has been estimated the intensity of scattered photons under the peak in the net spectrum of the Detector, by dividing the number of events in the peak (through a gaussian fit) for the acquisition time. We obtained a total number of events in the net spectrum of $\Sigma_{\gamma,tot} = (8.2 \pm 0.1) \cdot 10^3$ and, re-scaling by the time, an intensity of $\Sigma_\gamma = \frac{\Sigma_{\gamma,tot}}{t_{acq}} = (0.190 \pm 0.002) s^{-1}$.

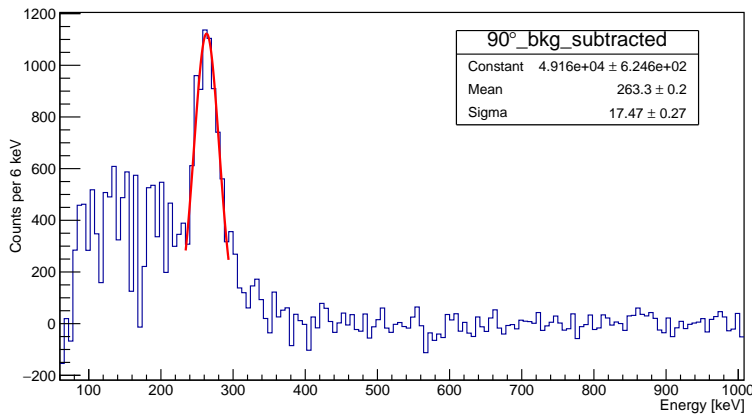


Figure 13: Net spectrum of scattered photons at 90° for an acquisition time of 12 hours.

7.4 Comparison between experimental and theoretical cross sections

Using Eq. 1 in the case of a scattering angle $\theta = 90^\circ$ and an incident photon $E_\gamma = 511 keV$ we expect a scattered photon with energy $E_{\gamma'} = \frac{E_\gamma}{2}$. The theoretical cross section becomes:

$$\left[\frac{d\sigma(\Theta_f)}{d\Omega} \right]_{th} = \frac{3r_e^2}{16} \quad (13)$$

The cross section uncertainty depends only on the angular position of the Detector σ_θ since the other parameters have negligible errors. The energy $E_{\gamma'}$ of the scattered photons depends on the angle θ too, so by inserting $E_{\gamma'}$ of Eq. 1 in Eq. 2 we obtained:

$$\sigma_{cs}^{th} = \frac{r_e^2}{2} \left(\frac{E_{\gamma'}}{E_\gamma} \right)^2 \left[\frac{E_{\gamma'}}{m_e c^2} \left(3 \frac{E_{\gamma'}}{E_\gamma} + \frac{E_\gamma}{E'_\gamma} - 2 \sin^2 \theta \right) + \cos(\theta) \right] \sin(\theta) \sigma_\theta \quad (14)$$

For $\theta = 90^\circ$ the theoretical uncertainty becomes:

$$\sigma_{cs,90}^{th} = \frac{3r_e^2}{32} \sigma_{\theta=90^\circ} \quad (15)$$

$\Delta\Omega_f$	N	ϵ	$\frac{I}{S}$	Σ_γ
$(0.041 \pm 0.001)sr$	$(6 \pm 1) \cdot 10^{24}$	$(67.8 \pm 0.1)\%$	$(2.6 \pm 0.1) \cdot 10^6 m^{-2}s^{-1}$	$(0.190 \pm 0.002)s^{-1}$

Table 4: Necessary experimental values to estimate the cross section.

From the parameters obtained in the previous sections (summarized in Tab. 4) we are able to estimate the experimental value of the cross section (in Eq. 17), considering as uncertainty:

$$\sigma_{cs}^{exp} = \left[\frac{d\sigma(\Theta_f)}{d\Omega} \right]_{exp} \sqrt{\left(\frac{\sigma_{\Sigma_\gamma}}{\Sigma_\gamma} \right)^2 + \left(\frac{\sigma_\epsilon}{\epsilon} \right)^2 + \left(\frac{\sigma_{\Delta\Omega_f}}{\Delta\Omega_f} \right)^2 + \left(\frac{\sigma_I}{I} \right)^2 + \left(\frac{\sigma_S}{S} \right)^2 + \left(\frac{\sigma_N}{N} \right)^2} \quad (16)$$

$$\frac{d\sigma(\Theta_f)}{d\Omega}_{th} = (1.5 \pm 0.1) \cdot 10^{-2} b \quad \frac{d\sigma(\Theta_f)}{d\Omega}_{exp} = (4.5 \pm 0.8) \cdot 10^{-3} b \quad (17)$$

The difference between the two values can be partially justified in terms of geometrical considerations. The intensity of the photons which impinge on the the aluminium sample producing a 511 keV peak on the Tagger was estimated through the relation $\epsilon \cdot N_{Scaler} \cdot F(511)$. However, the photopeak efficiency ϵ was calculated in a configuration where the Detector was completely absorbing the photons coming from the collimator (Sec. 7.1). As the measurement was made, the aluminium sample covers a fraction of this solid angle (Fig. 14). Observing the geometry of the system, it was estimated the total surface S_{tot} at the same distance from the source of the aluminium sample, which the emitted photons can reach without being shielded. From the ratio between the surface of the aluminium sample S_{Al} and the latter, it is estimated how much the photopeak efficiency must be corrected. We get:

$$\epsilon' = \frac{S_{Al}}{S_{tot}} \epsilon \simeq \frac{1}{2} \epsilon \quad \Rightarrow \quad \frac{d\sigma(\Theta_f)}{d\Omega}_{exp} (\epsilon') = (9.0 \pm 1.5) \cdot 10^{-3} b$$

8 Conclusions and perspectives

In this work, we experimentally verified the Compton scattering relation at different angles and we compared the experimental value of the Klein Nishina differential cross section with respect to the experimental one at 90° . We observed, however, that the nominal angular positions don't correspond to the that observed and the experimental results are biased. We tried to obtain a realistic estimation of the real detected angle and its statistical uncertainty by simulating the interaction process with a simple 2D model based on the experimental geometry. This model can approximately explain what happens and it allows to get reasonable errors.

The main problem in this experiment was the geometry: in particular the large volume of the Detector and the Scatterer. A possible solution consists in positioning the Detector at longer distances. However, for greater distances, a longer acquisition time is required (with higher environment noise). Another possibility is to use a source with higher activity and smaller volume detectors.

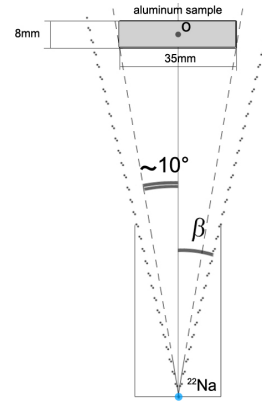


Figure 14: Alluminum sample